Depth variation of the mid-mantle seismic discontinuity

Fenglin Niu & Hitoshi Kawakatsu

Earthquake Research Institute, the University of Tokyo

Abstract. Short-period array seismograms of deep events that occurred in the Indonesia, Japan and Izu-Bonin arcs are stacked and beam-formed to identify the near-source S-P converted waves that result from the mantle transition discontinuities. Most of the resulting images reveal the existence of a mid-mantle seismic discontinuity ("920 km discontinuity") in these regions. Of the 15 events analyzed, three that occurred at the western end of the Indonesia arc show clear S-P arrivals observable even in individual seismograms. The mid-mantle discontinuity is characterized by large depth variation (900 ~ 1080 km) and velocity contrast variation in different subduction zones. Especially, the depth variation of the mid-mantle discontinuity beneath the Indonesia arc, where the discontinuity deepens from 940 km at the eastern end to 1080 km at the western end, appears to be well correlated with the location of the high-velocity anomalies in recent tomographic models. However, the mid-mantle discontinuity cannot be simply coincided with the bottom of the high-velocity anomalies, because a velocity increase at the discontinuity is observed from the waveform analysis.

Introduction

Recent tomographic studies in the western Pacific region [*Zhou and Clayton*, 1990; *van der Hilst et al.*, 1991; *Fukao et al.*, 1992; *Sakurai et al.*, 1995] have found that high-velocity anomalies [hereafter referred to as HVAs] are deflected at the '660-km' discontinuity in some subduction zones and extend to at least several hundred kilometers below the '660-km' discontinuity, but no deeper than approximately 1100 km, in others. This feature is clearly shown in recent studies of the correlation between seismic tomography and subduction history [*Wen and Anderson*, 1995; *Kývalová et al.*, 1995]. The result of tomographic studies showing that subducted slabs are trapped in the depth range of 800-1100 km suggests that there may exist a geodynamical boundary at this depth which resists slabs penetration. Meanwhile, we have reported that a mid-mantle seismic discontinuity exists at a depth of about 920 km beneath Tonga and two other subduction zones [*Kawakatsu and Niu*, 1994]. Therefore the nature of this "920 km discontinuity" may have significant implication for mantle dynamics; further detailed study of the "920 km discontinuity" in different subduction zones to delineate its relation with the HVAs appears to be essential.

In this paper, we extend our earlier study [*Kawakatsu and Niu*, 1994] to identify near-source S-P converted waves ($S_{660'}P$, $S_{920'}P$) in short-period seismograms of deep events in the Indonesia, Japan and Izu-Bonin arcs subduction zones. We find that the depth variation of the "920 km discontinuity" is much larger than we had originally thought. In the rest of this paper we therefore refer to this feature as a mid-mantle discontinuity.

Array Analyses

We used all earthquakes with depth $\geq$ ~350 km that occurred in the Indonesia, Japan and Izu-Bonin arcs from January 1990 to December 1994, for which high quality array data (e.g., J-array [*J-array Group*, 1993]) are available. The data used for the eight Indonesia arc events are short-period seismograms from the J-array. For the Japan and Izu-Bonin arc events, we use short-period seismograms from the Southern California Seismographic Network (SCSN). Because the SCSN seismograms usually cover only several tens of seconds after the direct P wave, we chose seven deep events with a record length longer than 60 sec so that we could see the later-arriving phases. Source parameters of the events used are listed in Table 1. We read the pP phase from the global broadband network of IRIS and redetermine the hypocentral depths. The source depth accuracy primarily depends upon the proper identification of pP, and, in general, an accuracy of ±10km in hypocentral depth estimate is expected. Since clear S-P converted waves were identifiable even in most of the individual seismograms for the three earthquakes that occurred at the western end of the Indonesia arc, we will mainly concentrate on the results of array analysis of those events in the following. Results for the Japan and the Izu-Bonin arcs events are available from Table 1.

Indonesia Events Fig. 1a shows the raw waveforms recorded by the J-array for a deep event that

Table 1. Earthquakes Used and Parameters Estimated

Date (y m dy)	Time (h min s)	Lat.	Lon.	Depth km	Region	Mag. mb	'660' km	'920' km	$\frac{S_{920'}P}{S_{660'}P}$
1990 08 27	15 17 12.7	-6.86	125.41	512.1	Banda Sea	5.8	670.	940.	0.35
1991 06 07	11 51 27.6	-7.26	122.57	543.0	Flores Sea	6.8	720.	945.	0.34
1992 08 02	12 03 20.2	-7.12	121.72	498.3	Flores Sea	6.6	710.	950.	0.33
1992 09 02	05 50 02.5	-6.04	112.14	636.5	Java	6.6	720.	1020.	0.64
1992 12 27	21 49 05.4	-6.11	113.06	621.5	Java	5.9	†	†	
1994 09 28	16 39 52.0	-5.67	110.46	638.0	Java Sea	5.8	740.	1080.	0.78
1994 09 28	17 33 59.1	-5.57	110.42	634.0	Java Sea	5.4	740.	1080.	0.78
1994 11 15	20 18 11.3	-5.60	110.23	570.0	Java Sea	6.2	720.	1080.	*
1990 05 11	13 10 20.3	41.78	130.88	586.0	Japan Sea	6.2	-	-	
1993 01 19	14 39 26.4	38.57	133.52	454.0	Japan Sea	6.0	660.	943.	0.22
1990 04 11	20 51 12.7	35.45	135.48	367.0	Honshu	6.0	†	†	
1993 10 11	15 54 22.3	31.99	137.89	365.0	Izu-Bonin	6.3	655.	-	
1992 10 30	02 49 49.4	29.97	138.93	408.0	Izu-Bonin	6.4	655.	970.	0.10
1990 08 05	01 34 57.5	29.51	137.60	614.0	Izu-Bonin	6.4	-	-	
1992 01 20	13 37 04.1	27.96	139.33	512.0	Izu-Bonin	6.6	655.	970.	0.25

- : Not observed; †: Not observed due to unfavorable source mechanism.
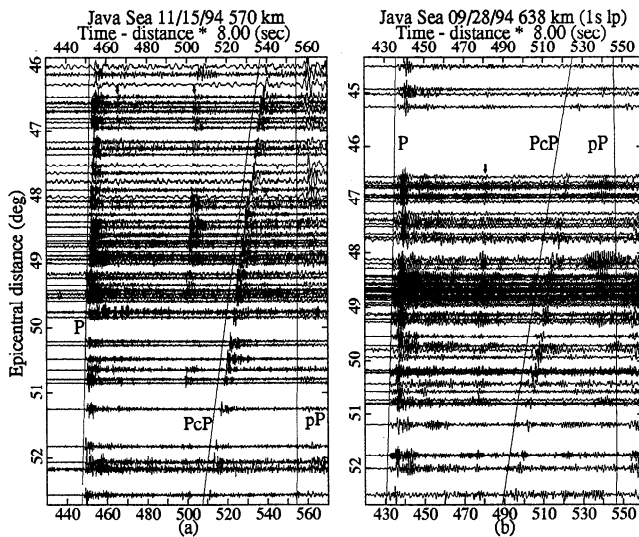*: 0.65 below 0.5 Hz; 1.87 in 0.5~1 Hz.

Fig. 1 (a) A portion of the seismic section for the 11/15/94 event. Theoretical travel times of the iasp91 model [Kennett and Engdahl, 1991] for the major expected body wave arrivals are indicated by straight lines. Note that two clear phases at 15 and 50 sec after the direct P arrival (indicated by arrows) can be recognized in most of the individual seismograms. (b) Same as (a) for the larger of 09/28/94 events, low-pass filtered at a cut-off period of 1 sec. Note that a clear phase appears at 40 sec after the direct P wave, an interval approximately 10 sec shorter than in (a).

occurred on November 15, 1994, plotted in order of increasing epicentral distance. Between the arrivals of the direct P and PcP, two conspicuous signals at about 15 and 50 sec (especially the latter) after the direct P arrival line up very well. To identify these phases, we used stacking and beam-forming to determine the incidence angle and azimuth of the arrivals. The data were low-pass filtered at a cut-off period of 2 sec before stacking and beam-forming.

Linear stacking   Before stacking the data, we first aligned the seismograms such that the maximum amplitude of the direct P, which is normalized to unity, occurs at time zero. We employed a time window of 150 sec for the J-array data. For the SCSN data, shorter time windows, though not less than 60 sec, were used due to limitations of the available record length. Records from approximately 40 to 120 stations were selected for a linear stacking process. Details of the stacking procedure are given by Kawakatsu and Niu [1994]. Fig. 2 shows the result of the linear stacking for the records shown in Fig. 1a; the black clusters represent greater energy, indicating potential phase arrivals. The two later arrivals seen in Fig. 1a have slowness slightly less than that of the direct P wave (defined to be zero), which is characteristic of S-P conversion waves. The signals at about 22 and 38 sec have slowness slightly larger than that of the direct P wave, and are identified as the reflected waves ($p_{410'}P$, $s_{410'}P$) at the '410-km' discontinuity, which is 10 km deeper than the global average. At the bottom of Fig. 2, we also show the stacked waveforms of the observed and synthetic data at a slowness of -0.3 s·deg^{-1}, at which the $S_{1080}P$ reaches its peak. The
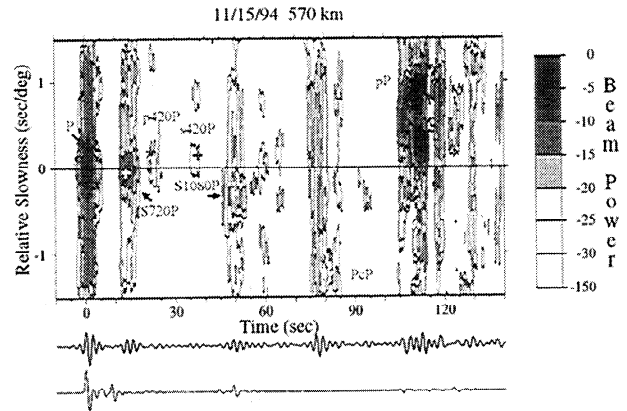

Fig. 2 (top) Normalized amplitudes of linear stacked waveforms is plotted as a function of relative slowness and arrival time. The expected arrivals of the later phases are indicated by crosses. (bottom) Stacked waveforms of the observed and synthetic data at a slowness of -0.3 s·deg^{-1}.

reflectivity synthetic seismograms [Kennett, 1988] are calculated using the Harvard CMT solution for a modified iasp91 model, which has an extra discontinuity at a depth of 1080 km; both the velocity and density contrasts are assumed to be 55% of those at the '660-km' discontinuity.

Beam-forming   In the linear stacking we assumed that the ray path stays in the same great circle plane as that of the direct P wave, and determined the incidence angle (i.e., slowness) of the signals in different time windows. We check this assumption by applying beam-forming to several individual time windows. We first align the filtered seismograms so that the direct P arrivals coincide with the theoretical iasp91 travel-time. We vary the slowness from 4 to 10 s·deg^{-1} at increments of 0.1 s·deg^{-1}, and the azimuth is deviated from the great circle within a range of ±40° at increments of 5°. Then we calculate the energy of the stacked seismogram for each slowness and azimuth within a time window of 4 sec.
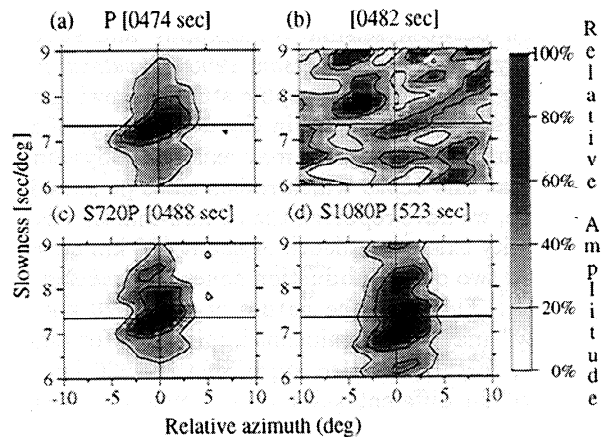

Fig. 3 Beam amplitudes are shown as a function of slowness and azimuth. (a) direct P wave; (b) P-coda scatters; (c) $S_{720}P$; (d) $S_{1080}P$. Numbers on top of each figure indicate the time in sec from the origin time, the time window used in the analysis being 4 sec.

Fig. 3 shows the result of the beam-forming for the 11/15/94 event; the position of the peak of contours represents the most likely slowness and azimuth of each arrival. The intersection of the two straight lines is the expected position of the direct P wave. The resolvability of the slowness and azimuth provided by the array may be visually assessed from the beam-forming result for the direct P wave. The energy in the time window 8 sec after the direct P is diffused over both slowness and azimuth, suggesting that the arrivals in this time window are mainly scattered waves. But in the time windows where the S-P converted waves are expected to arrive, most of the energy comes from the great circle azimuth with a slowness slightly smaller than that of the direct P wave. This rules out the possibility that these arrivals are scattered energy from unresolved inhomogeneities in the mantle.

The incidence angle and back azimuth determined by using the above methods suggest that the well-aligned signals shown in Fig. 1a are S-P waves converted at mantle discontinuities beneath the source. From the travel-time difference with the direct P wave, we estimate the conversion depths to be about 720 and 1080 km, respectively.

Two more deep earthquakes occurred on September 28, 1994 at almost the same epicentral location as the 11/15/94 event but at different hypocentral depths (Table 1). The J-array records for these two events are very similar due to the almost identical focal mechanisms. In Fig. 1b we show the waveforms for the larger of the two events. We can observe clear S-P converted waves in Fig. 1b; however, the well-aligned later arrivals appear 40 sec after the direct P wave, approximately 10 sec

earlier than the value of 50 sec observed for the event of 11/15/94 (Fig. 1a). Since the hypocentral depth of the former event is about 70 km deeper than the latter, the S-P conversion depths for the two events on 09/28/94 are again estimated at about 1080 km. The good agreement of the conversion depths for these three events further confirms our identification of the phases and strongly suggest that beneath the western end of the Indonesia arc the mid-mantle discontinuity is depressed to a depth of 1080 km.

Discussion

The observed amplitude of $S_{1080}P$ for the three events that occurred at the western end of the Indonesia arc is highly frequency dependent. In the low-frequency band of less than 0.5 Hz, the relative amplitude of $S_{1080}P$ to $S_{720}P$ is about 0.7; the relative amplitude increases to nearly 1.9 in the frequency range of 0.5~1 Hz. We do not observe such obvious frequency dependence for the other events. We calculated the S-to-P conversion coefficient of a plane wave for discontinuities with different transition thickness using the Thomson-Haskell method. A sharp discontinuity with a thickness less than 5 km and a velocity jump of about 55% of that of the '660-km' discontinuity can explain the observed frequency dependence of the relative amplitude ratio of $S_{1080}P$ to $S_{720}P$, if we assume that the '660-km' discontinuity has a thickness of about 10 km.

Although it is often very difficult to measure the polarity of later arrivals in high frequency data, we suggest that the polarity of $S_{1080}P$ is positive. Fig. 4 compares P, $S_{1080}P$, and S_cP waveforms of the raw vertical component seismograms at relatively noise-free J-array stations. The apparent positive polarity of $S_{1080}P$ can be confirmed by comparing the waveform with other clearly observed phases; we use S_cP for this purpose, because the direct P goes through near the nodal line and is not suitable for the waveform comparison. The strong similarity of $S_{1080}P$ and S_cP waveforms indicates that the polarity of these two phases is the same. Since the polarity of S_cP is expected to be positive due to the known focal mechanism, we conclude that the polarity of $S_{1080}P$ is also positive. This polarity together with the known focal mechanism requires a velocity increase at a depth of 1080 km in this area, if the observed phase is an S to P converted phase.

A systematic investigation of the eight deep events in the Indonesia arc clearly shows that beneath the eastern end of the Indonesia arc, the mid-mantle discontinuity has a depth of about 940 km; it steadily goes deeper to a depth of 1080 km at the western end of the arc (Fig. 5) Analysis of the seven deep events in the Japan and Izu-Bonin arcs also reveals the depth variation of the mid-mantle discontinuity, which has a smaller velocity contrast in these regions; it has a depth of 945 km beneath the Japan sea and deepens to a depth of 970 km beneath the Izu-Bonin arc (Table 1).

At the bottom of Fig. 5, we show a tomographic model of the seismic velocity structure of *Sakurai et al.*
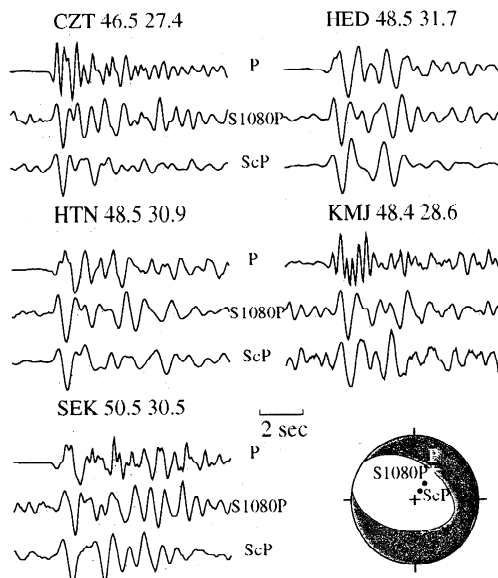

Fig. 4 Vertical raw waveforms of P, $S_{1080}P$, and S_cP for the 11/15/94 event at different stations are shown together with the corresponding Harvard CMT solution (lower hemisphere). This event appears to have two subevents with different focal mechanisms separated in time by few seconds. Note the strong similarity between $S_{1080}P$, and S_cP waveforms.
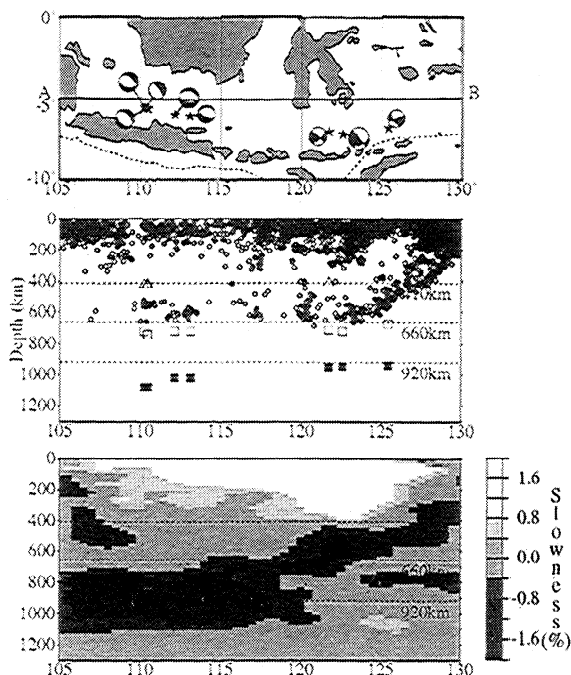
Fig. 5 (*top*) Geographic distribution of the eight deep events that occurred in the Indonesia arc. (*middle*) Conversion points are shown in the vertical cross section (line AB) along the Indonesia arc. Earthquake locations from ISC (1964~1991) are also shown. Open and closed squares stand for the S-P conversion points of $S_{660'}P$ and $S_{920'}P$, respectively. Open triangles are the reflection points of $p_{410'}P$ or $s_{410'}P$. (*bottom*) Whole mantle P wave tomographic image of the same cross section, after *Sakurai et al.* [1995].

[1995] on the same vertical cross-section. The location of the HVAs beneath the western part of the Indonesia arc is deeper than that at the eastern end. This is in good general agreement with the trend of depth variation of both the mid-mantle and '660-km' discontinuities. The intense HVA beneath Borneo island is one of the strongest in the mid-mantle and has consistently inferred by recent tomographic studies using different data sets [e.g., *Li and Romanowicz*, 1996]. So it seems likely that the deepening of the discontinuities toward the western end of the Indonesia arc is related to the HVA. Note, however, that the mid-mantle discontinuity cannot be simply coincided with the bottom of the HVA as was suggested in our earlier paper as one possible explanation [*Kawakatsu and Niu*, 1994], because a velocity decrease would be expected in that case.

Because of the lack of an appropriate deep earthquake between longitude of 115° and 120° during the time period of our study, the continuity of the mid-mantle discontinuities from the eastern end to the western end beneath the Indonesia arc should not be considered proved. However, if we assume that this feature is continuous, the observations presented in this paper suggest that the mid-mantle discontinuity corresponds to a velocity increase. A regional variation of the depth, velocity contrast, and sharpness of the mid-mantle discontinuity has also been observed.

No obvious explanation for such a feature in the mid-mantle below the '660-km' discontinuity seems to exist in currently available geophysical literatures. Further seismological studies in the western Pacific region, where many HVAs appear to exist in the mid-mantle [*Sakurai et al.*, 1995], may be the key to resolve this puzzling situation. The mantle structure below the '660-km' discontinuity down to at least ~1100 km appears to be more complicated than generally expected [*Kawakatsu and Niu*, 1994; *Niu and Kawakatsu*, 1996].

References

Fukao, Y., M. Obayashi, M. Inoue, and M. Nenbai, Subducting slabs stagnant in the mantle transition zone, *J. Geophys. Res.*, *97*, 4809-4822, 1992.

J-Array Group, The J-Array program: system and present status, *J. Geomag. Geoelectr.*, *45*, 1265-1274, 1993.

Kawakatsu, H., and F. Niu, Seismic evidence for a 920-km discontinuity in the mantle, *Nature*, *371*, 301-305, 1994.

Kennett, B. L. N., Systematic Approximations to the Seismic Wavefield, in *Seismological Algorithms*, edited by D. J. Doornbos, pp. 237-259, Academic Press, 1988.

Kennett, B. L. N., and E. R. Engdahl, Travel times for global earthquake location and phase identification, *Geophys. J. Int.*, *105*, 429-465, 1991.

Kývalová, H., O. Čadek, and D. A. Yuen, Correlation analysis between subduction in the last 180 Myr and lateral seismic structure of the lower mantle: Geodynamic implications *Geophys. Res. Lett.*, *22*, 1281-1284, 1995.

Li, X.-D., and B. Romanowicz, Global mantle shear-velocity model developed using nonlinear asymptotic coupling theory, *J. Geophys. Res.*, *101*, 22245-22272, 1996.

Niu, F., and H. Kawakatsu, Complex structure of the mantle discontinuities at the tip of the subducting slab beneath the northeast China: a preliminary investigation of broadband receiver functions, *J. Phys. Earth*, *44*, 701-711, 1996.

Sakurai, T., M. Obayashi, and Y. Fukao, Tomographic image of slab and mantle plume, *Program and Abstracts, Seism. Soc. Japan*, *1*, 624, 1995 (in Japanese).

van der Hilst, R., R. Engdahl, W. Spakman and G. Nolet, Tomographic imaging of subducted lithosphere below north-west Pacific island arcs, *Nature*, *353*, 37-43, 1991.

Wen, L., and D. L. Anderson, The fate of slabs inferred from seismic tomography and 130 million years of subduction, *Earth Planet. Sci. Lett.*, *133*, 185-198, 1995.

Zhou, H.W., and R. W. Clayton, P and S wave travel time inversions for subducting slab under the island arcs of Northeast Pacific, *J. Geophys. Res.*, *95*, 6829-6851, 1990.

Fenglin Niu and Hitoshi Kawakatsu,
Earthquake Research Institute, the University of Tokyo
1-1-1 Yayoi, Bunkyo-ku, Tokyo 113, Japan.
(e-mail [niu,hitosi]@eri.u-tokyo.ac.jp)